INDERSCIENCE PUBLISHERS
Linking academia, business and industry through research

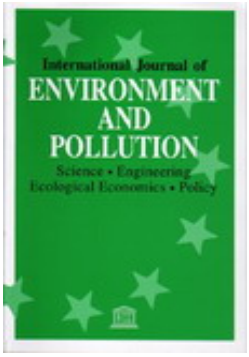

International Journal of Environment and Pollution

ISSN online: 1741-5101 - ISSN print: 0957-4352
https://www.inderscience.com/ijep

Industrial chain technology paths and economic feasibility of agricultural waste resource utilisation

Lei Xu, Cheng Cheng, Ya'nan Zhang, Yuanlin Wang, Menglin Ni

DOI: 10.1504/IJEP.2025.10074876

Article History:

Received:	14 April 2025
Last revised:	07 July 2025
Accepted:	24 October 2025
Published online:	05 January 2026

Industrial chain technology paths and economic feasibility of agricultural waste resource utilisation

Lei Xu

School of Business Administration,
Shandong Women's University,
Jinan, 250300, Shandong, China
Email: lxxu07@sdwu.edu.cn

Cheng Cheng

School of Marxism,
Shandong University of Chinese Traditional Medicine,
Jinan, 250300, Shandong, China
Email: 60080036@sdutcm.edu.cn

Ya'nan Zhang

Graduate School,
Central University of Finance and Economics,
Haidian, 100081, Beijing, China
Email: zhangyanan2011@cufe.edu.cn

Yuanlin Wang

Department of Auditing,
Weifang University,
Weifang, 261061, Shandong, China
Email: 20190070@wfu.edu.cn

Menglin Ni*

School of Business Administration,
Shandong Women's University,
Jinan, 250300, Shandong, China
Email: 30081@sdwu.edu.cn
*Corresponding author

Abstract: In response to the high cost and insufficient coordination of the industrial chain in the utilisation of agricultural waste, this paper constructs an optimisation scheme for the coordinated scheduling of biocatalysis and digital twins. By screening heat-resistant β-glucosidase mutants and establishing straw-enzyme adaptation rules, combined with microwave-ultrasonic pretreatment and near-infrared (NIR), the conversion efficiency is improved. The virtual industrial chain model integrates graph convolutional networks (GCN) to predict raw material fluctuations, and improves the non-dominated

sorting genetic algorithm II (NSGA-II) algorithm to achieve Pareto optimality of transportation and equipment utilisation. Experiments show that the reducing sugar yield of the mutant enzyme system reaches 90.2% in 72 h; the path optimisation rate of the scheduling system exceeds 0.8 within 12 months, and the equipment idle loss is controlled at 21,000–23,000 US dollars, which significantly improves the efficiency of resource utilisation.

Keywords: agricultural waste; resource utilisation; industrial chain technology path; economic feasibility; digital twin model; GCN; graph convolutional networks; NSGA-II; non-dominated sorting genetic algorithm II.

Reference to this paper should be made as follows: Xu, L., Cheng, C., Zhang, Y., Wang, Y. and Ni, M. (2025) 'Industrial chain technology paths and economic feasibility of agricultural waste resource utilisation', *Int. J. Environment and Pollution*, Vol. 75, No. 4, pp.361–387.

Biographical notes: Lei Xu is a Faculty of Shandong Women's University. He received his Master's and Doctor's degree Saitn Mary's University of Minnesota. His research field includes rural enterprise management and agricultural product supply chain.

Cheng Cheng is a Faculty at Shandong University of Traditional Chinese Medicine. She received her Bachelor's degree from Shandong Jianzhu University and her Master's degree from the Party School of the CPC Shandong Provincial Committee. Currently, her research interests include the history of the Communist Party of China.

Ya'nan Zhang is an Assistant Research Fellow at Central University of Finance and Economics. She received her Bachelor's degree from Shandong University, her Master's degree from Renmin University of China. Her academic research focuses on educational economics and management and educational leadership and management.

Yuanlin Wang is an Accountant in Weifang University. She received her Bachelor's degree from Qingdao University, her Master's degree from Qingdao University. Her research interests include accounting and auditing.

Menglin Ni graduated from the University of Exeter and works in School of Business Administration, Shandong Women's University. Her research interests include agriculture and business management.

1 Introduction

The resource utilisation of agricultural waste is an important practical direction for the circular economy and sustainable development. Biomass such as straw and fruit shells is rich in cellulose, hemicellulose, and lignin, which can be used to prepare high-value-added products, such as biofuels, organic acids, and functional materials through biocatalysis (Gröger et al., 2022; Hanefeld et al., 2022) and thermochemical conversion (Jha et al., 2022; Choi et al., 2023). The optimisation of technology paths must consider conversion efficiency, energy consumption control, and the coordination of the industrial chain. Economic feasibility is affected by factors such as raw material collection costs, process stability, and policy subsidies (He, 2024; Lama and Karmakar, 2025). In this

context, systematic research on the technical integration and economic benefits of waste resource utilisation is of key significance to promoting green manufacturing and low-carbon agriculture.

Research on the resource utilisation of agricultural waste still faces multi-dimensional challenges. In the biotransformation process, there is a significant difference between enzyme catalytic efficiency and substrate compatibility. Existing enzymes have a limited ability to degrade complex biomass structures. There is a lack of systematic guiding rules for mutant screening, making it difficult for saccharification rates to break through the industrial threshold (Mengqi et al., 2023; Peng et al., 2023a). The energy consumption of the pretreatment process and the product inhibition effect form a technical paradox. Although conventional physical and chemical methods can improve substrate accessibility, the accumulation of byproducts inhibits the efficiency of subsequent enzymatic hydrolysis (Capanoglu et al., 2022; Gupta et al., 2023). The bottleneck at the level of industrial chain coordination is more prominent. The supply of raw materials is highly heterogeneous in time and space. The existing scheduling models mostly rely on static parameters and cannot dynamically respond to seasonal fluctuations and market changes (Panasenko et al., 2022; Gupta et al., 2022). The trade-off between transportation costs and equipment utilisation has not yet established a quantitative decision-making mechanism, and empirical production scheduling has led to resource mismatch (Phiri et al., 2023; Toma et al., 2024). In terms of economic evaluation, existing models do not adequately consider the value of externalities, such as carbon trading revenue and policy subsidies, and it is difficult for static financial analysis to reflect the actual investment return cycle (Khanal et al., 2024; Khalid et al., 2023). The application of digital technology is still at the stage of single-point optimisation. There is a lag in data collection during the biological reaction process, and there is parameter drift between virtual simulation and actual production. The prediction precision of the twin model is limited by the ability to integrate multi-source heterogeneous data (Madhu et al., 2023; Meraj et al., 2023). The optimisation efficiency of intelligent algorithms under complex constraints is insufficient, and local optimal solutions cannot meet the coordination needs of the entire chain. These factors jointly restrict the large-scale application and commercial promotion of agricultural waste resource technology (Peng et al., 2023b; Zhu et al., 2025).

This paper aims to construct a full-chain coordinated optimisation framework for the resource utilisation of agricultural waste, breaking through the key bottlenecks of existing technologies in terms of conversion efficiency, system integration, and economic feasibility. The core contribution is to propose a 'biocatalysis-digital twin' dual-driven strategy to achieve cross-level optimisation from the molecular scale to the industrial scale. At the biotransformation level, an enzyme-substrate adaptation rule library based on structural biology is established. The structure-activity relationship between the supramolecular structure of cellulose and the enzymatic hydrolysis efficiency is analysed through molecular dynamics simulation. A mutant enzyme system with directed evolution characteristics is developed. The microwave-ultrasonic coupled field control technology is innovatively applied and combined with online spectral analysis to build a closed-loop feedback system for the pretreatment process, thus achieving dynamic optimisation of reaction parameters. In terms of industrial chain coordination, a virtual twin model with multi-dimensional parameters is constructed, integrating 37 key factors in four modules: raw material properties, equipment operation, environmental constraints, and market dynamics. Graph convolutional networks (GCN) are used to capture the

spatiotemporal correlation features of the supply chain. An intelligent decision-making engine based on a multi-objective evolutionary algorithm is adopted to establish a quantitative balance mechanism between transportation costs, equipment utilisation, and carbon emissions. The economic evaluation model breaks through the limitations of static analysis, embedded with the carbon trading price fluctuation function and the policy subsidy dynamic adjustment module. A full life cycle evaluation method that considers the value of externalities is also proposed. The research results provide a system solution that combines advanced biotechnology and digital intelligence for the high-value utilisation of agricultural waste, promoting the circular economy model from the laboratory to industrialisation.

2 Related work

Existing research has explored agricultural waste resource technology in multiple dimensions. In bioconversion, some studies have improved the thermal stability of cellulase through directed evolution technology to improve the efficiency of straw saccharification (Zhang et al., 2022; Koksharov et al., 2022). Srivastava et al. (2024) used alkali-pretreated orange peel waste for solid-state fermentation to optimise the yield of fungal cellulase and achieve the highest enzyme activity under optimal conditions. Nickel cobaltate nanoparticles improved the stability of the enzyme and the hydrolysis efficiency of alkali-pretreated rice husks, showing potential for industrial application. The steam explosion pretreatment process developed by some studies has increased the removal rate of hemicellulose (Alizadeh et al., 2022; Pažitný et al., 2022). Semwal et al. (2024) optimised the conditions for water- and dilute acid-assisted steam explosion treatment of rice straw, which increased the glucose conversion rate and reduced enzyme consumption. By controlling the temperature and adding dilute acid, the sugar recovery rate and ethanol yield were increased, reaching up to 222 L/ton of rice straw. In terms of industrial chain coordination, some studies have constructed a raw material collection optimisation model based on a geographic information system (GIS) to reduce transportation costs (Yalcinkaya and Uzer, 2022; Ali et al., 2023). Fawad et al. (2022) combined the analytic hierarchy process and GIS methods to evaluate the suitability of waste collection and disposal in the Mohmand marble area in Pakistan to reduce ecological hazards and social concerns. He proposed that priority should be given to protecting water bodies and agricultural land and to providing decision support for waste management site selection. Existing research focuses on optimising a single link and lacks a coordinated perspective of the entire chain. The performance improvement of enzymes often ignores the compatibility with pretreatment processes. The application of digital technology mostly stays in static scheduling (such as fixed transportation routes), making it difficult to cope with real-time supply and demand fluctuations. The existing scheduling models are mostly dependent on static parameter settings, which makes it difficult to adapt to the spatial and temporal heterogeneity and dynamic fluctuation of agricultural waste supply, and lack of effective support for multi-objective collaborative optimisation. Economic feasibility studies often use static cost models, which do not fully consider the value of externalities, such as carbon trading income, resulting in investment return predictions that deviate from reality.

In view of the limitations of enzyme performance and supply chain coordination, recent studies have attempted to seek breakthroughs through interdisciplinary technology integration. In biocatalysis, molecular docking technology is used to predict enzyme-substrate binding energy (Åqvist and van der Ent, 2022; Zheng et al., 2023), and microwave-ultrasonic coupled pretreatment can reduce energy consumption (Cai et al., 2024; Li et al., 2023). In digitalisation, the digital twin technology has begun to be applied to the dynamic control of bioreactors (Park et al., 2023; Hill et al., 2024), and GCN neural networks have also been used for supply chain demand prediction (Tu et al., 2024; Liang et al., 2025). Rui and Li (2024) proposed a hybrid model that integrates GCN, long short-term memory (LSTM), and an attention mechanism. The accuracy of supply chain demand prediction was improved by integrating internet big data. The model optimised production planning and inventory management and reduced supply chain risks. However, these methods still have key flaws. Enzyme screening lacks substrate-specific adaptation rules, resulting in insufficient process stability. Digital models mostly use simplified parameters (fixed raw material components), making it difficult to reflect real production scenarios. Scheduling algorithms excessively pursue local optimality and fail to achieve multi-objective balance. This paper innovatively integrates biocatalytic modification and digital twin technology, and through the establishment of a three-level collaborative optimisation system of "enzyme-process-industry chain", systematically solves the problem of collaborative improvement of conversion efficiency and economic benefits.

3 Methods

Figure 1 presents the intelligent technology system of the agricultural waste resource utilisation industry chain, which includes five core modules: data layer, processing layer, digital twin layer, optimisation layer, and output layer. The data layer integrates the Carbohydrate-Active Enzymes Database (CAZy), real-time NIR spectroscopy monitoring data, and supply chain Internet of Things (IoT) sensor data stream. The processing layer obtains thermostable β-glucosidase mutants through Rosetta design-energy calculation (Rosetta Delta Delta G, RosettaDDG) screening. Combined with the component-enzyme system matching rules established by partial least squares regression (PLSR), the microwave-ultrasonic coupled pretreatment reactor is driven to optimise biomass conversion. A 37-dimensional parameter virtual model is constructed in the digital twin layer, and the GCN architecture is used to predict raw material supply fluctuations. An improved NSGA-II is deployed in the optimisation layer to achieve Pareto optimal scheduling between the dual objectives of transportation cost and equipment vacancy rate. The output layer ultimately achieves cost-optimised logistics and transportation and the commercialisation of high-purity bio-based products. Each module achieves closed-loop optimisation through a strict data interface, including real-time process parameter feedback, dynamic scheduling instruction transmission, and market supply and demand data interaction, forming a complete 'collection-pretreatment-conversion-sales' intelligent decision-making system.

Figure 1 Intelligent technology system of the agricultural waste resource utilisation industry chain

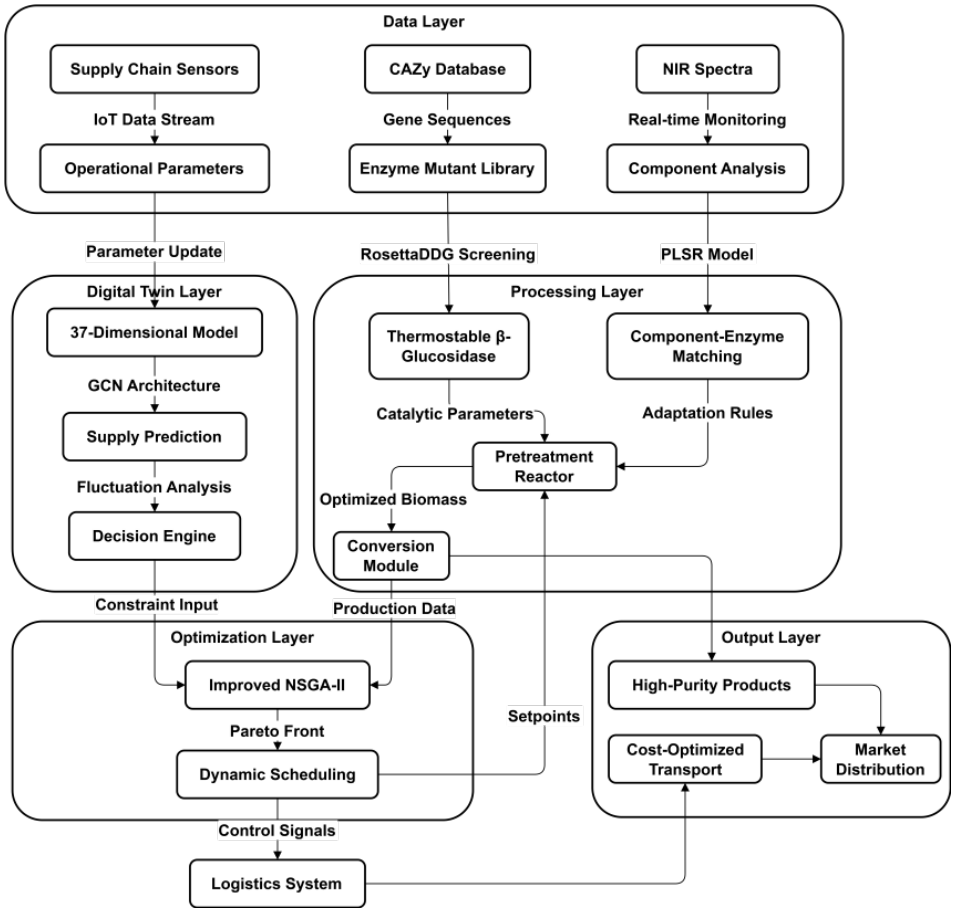

3.1 Biocatalyst directed screening system

Thermostable β-glucosidase mutants are screened out using the cellulase gene database and molecular docking technology, and the adaptation rules between straw components and enzyme systems are established.

3.1.1 Thermostable β-glucosidase mutant screening

The β-glucosidase sequences of glycoside Hydrolase Family 1 (GH1) and Glycoside Hydrolase Family 3 (GH3) are extracted from CAZy to construct a candidate set of 2145 homologous genes. The RosettaDDG algorithm is used to perform full-site mutation scanning on key residues in the active site (Tyr144, Glu165, and His228). The binding free energy change $\Delta\Delta G$ of the mutants is calculated. The screening threshold is defined as the joint optimisation objective of $\Delta\Delta G$ and the improvement in catalytic efficiency:

$$\begin{cases} \Delta\Delta G = G_{\text{mutant}} - G_{\text{wild-type}} \\ \dfrac{k_{\text{cat}}^{\text{mutant}} / K_{\text{m}}^{\text{mutant}}}{k_{\text{cat}}^{\text{wild-type}} / K_{\text{m}}^{\text{wild-type}}} \geq \alpha \end{cases} \tag{1}$$

Formula (1) is used to calculate the combined screening threshold of the binding free energy change ($\Delta\Delta G$) and the improvement in catalytic efficiency of β-glucosidase mutants, The selection of ΔΔG threshold and the catalytic efficiency improvement target is based on the physicochemical equilibrium mechanism of enzyme thermal stability and catalytic activity. The free energy change caused by protein mutation reflects the changing trend of structural stability. Although excessively large negative values can enhance thermal stability, they may limit the flexibility of active sites and affect substrate binding and catalytic efficiency. The joint optimisation target takes into account the needs of maintaining the stability of mutants in high-temperature environments and improving the reaction rate, ensuring their practicality and economy under complex industrial conditions. G is the binding free energy. α is the efficiency improvement threshold. $k_{\text{cat}}^{\text{mutant}}$ is the catalytic rate constant of the mutant enzyme, reflecting the maximum reaction rate. $K_{\text{m}}^{\text{mutant}}$ is the Michaelis constant of the mutant enzyme, reflecting the affinity of the enzyme for the substrate. $k_{\text{cat}}^{\text{wild-type}}$ and $K_{\text{m}}^{\text{wild-type}}$ are the corresponding parameters of the wild-type enzyme. The generalised Born solvation term uses default parameters, with a solvent dielectric constant of 78.5 and a solute-solvent contact distance of 0.2 nm.

Molecular docking is performed using AutoDock Vina 1.2.0. The substrate conformation library is generated by ConFabX. The force field parameters are selected from General Amber Force Field 2 (GAFF2). The binding energy calculation is optimised using an implicit solvation model.

$$\Delta G_{\text{bind}} = E_{\text{elec}} + E_{\text{vdW}} + G_{\text{GB}} + G_{\text{SA}} \tag{2}$$

Formula (2) is the implicit solvation model. ΔG_{bind} represents the binding energy between the mutant and the substrate. E_{elec} and E_{vdW} are the electrostatic and van der Waals energies, respectively. G_{GB} and G_{SA} are the generalised Born solvation and solvent accessible surface area terms. Molecular dynamics simulations are performed on the mutants that meet the constraints of the implicit solvation model to analyse the root mean square deviation (RMSD) of the active site and the stability of the hydrogen bond network.

Table 1 lists the comparative analysis of the energy compositions of wild-type β-glucosidase and mutant BglM7 during molecular docking. The molecular mechanics and generalised Born surface area method are used to calculate various energy terms, including electrostatic interaction energy, van der Waals interaction energy, generalised Born solvation free energy, and solvent accessible surface area energy terms. The data show that the mutant BglM7 exhibits better binding properties in all key energy terms. The electrostatic interaction energy is reduced by 3.5 kcal/mol, and the van der Waals interaction energy is reduced by 2.7 kcal/mol, indicating that its non-covalent binding ability with the substrate is significantly enhanced. Meanwhile, the changes in solvation effect-related terms (generalised Born solvation free energy and solvent accessible surface area energy) demonstrate that the mutant has better solvent adaptability. The

collaborative optimisation of these energy parameters confirms the improvement of the thermal stability and catalytic efficiency of the BglM7 mutant, providing a theoretical basis for its application in agricultural waste conversion.

Table 1 Molecular docking energy composition analysis

Energy composition	*Wild type* (kcal/mol)	*Mutant BglM7* (kcal/mol)	*Energy change* (kcal/mol)
Electrostatic interaction	–15.2	–18.7	–3.5
Van der Waals interaction	–24.6	–27.3	–2.7
Generalised born solvation free energy	12.4	10.8	–1.6
Solvent accessible surface area energy	3.2	2.9	–0.3

3.1.2 Straw component-enzyme system adaptation rule modelling

A multivariate response model of straw components (cellulose, hemicellulose, and lignin) and enzyme system activity is established. The sample set includes 356 straws. The components are determined using the NREL standard method. A feature matrix $\mathbf{X}$ is constructed. The enzymatic hydrolysis experiment is designed based on the Box-Behnken method. The response variable is $\mathbf{Y}$. The model is constructed using:

$$\mathbf{Y} = \mathbf{XB} + \mathbf{C} \tag{3}$$

$\mathbf{B}$ is the regression coefficient matrix. $\mathbf{C}$ is the residual term. The interaction effect is expanded by a second-order polynomial:

$$Y = \beta_0 + \sum_{i=1}^{3} \beta_i x_i + \sum_{i<j} \beta_{ij} x_i x_j \tag{4}$$

Y is the reducing sugar yield. β_0 is the model intercept. β_i is the linear term coefficient. x_i and x_j are the standardised component contents. β_{ij} represents the synergistic or antagonistic effect between components. i and j are used to index different straw components. The index of i corresponds to the three main components of cellulose, hemicellulose, and lignin.

The principal components of the feature matrix are extracted using principal component analysis (PCA). The enzyme system ratio M_p optimisation function is constructed:

$$\mathrm{M}_p = \min_{\mathbf{E}} \| \mathbf{PC} - \mathbf{WE} \|_F^2 + \lambda_m \| \mathbf{E} \|_1 \tag{5}$$

$\mathbf{PC}$ is the principal component matrix of the straw components. $\mathbf{W}$ is the enzyme activity weight matrix. $\mathbf{E}$ is the enzyme dosage sparse vector. λ_m controls the sparsity of enzyme dosage. $\| \cdot \|_F^2$ is the Frobenius norm. $\|\mathbf{E}\|_1$ is the L1 norm. The decision rule determines the optimal λ_m through cross-validation to ensure the nonlinear mapping precision of the enzyme system combination and straw components. The stability of the hydrogen bond network at the active site was analysed by molecular dynamics simulation, and the catalytic efficiency of mutants was determined experimentally.

Figure 2 reveals the synergistic regulatory mechanism of the cellulose and hemicellulose content of straw on the enzymatic hydrolysis rate. The spatial distribution of the enzymatic hydrolysis rate shows nonlinear characteristics, with its peak appearing in the component interval of about 52.5% cellulose and about 25% hemicellulose. This phenomenon is due to the substrate specificity and spatial accessibility of the cellulase system. As the main degradation target, the increase in cellulose content can increase the enzyme binding sites, but when it exceeds 52.5%, the dense crystalline region structure may limit the diffusion of enzyme molecules, resulting in a slowdown in the rate of growth. Hemicellulose exhibits a dual role. Its presence in an appropriate amount can maintain the porous structure of the straw and promote enzyme-substrate contact. When in excess, it significantly inhibits the hydrolysis efficiency by physically embedding cellulose and competitively adsorbing enzyme proteins. The steep decline in the surface area reflects the barrier effect of the lignin-hemicellulose complex on enzyme activity. This complex forms a physical barrier through hydrophobic interactions and hydrogen bond networks, making it difficult for cellulase to access the substrate. The asymmetric distribution of contour lines further shows that the inhibitory effect of hemicellulose on enzymatic hydrolysis is stronger than the promoting effect of cellulose, which is consistent with the specific recognition mechanism of cellulase active sites for β-1,4 glycosidic bonds. The consistency of the data and the model verifies the reliability of the component adaptation rules and provides a theoretical basis for the development of directed pretreatment processes.

Figure 2 Lignocellulose composition and enzymatic hydrolysis rate (see online version for colours)

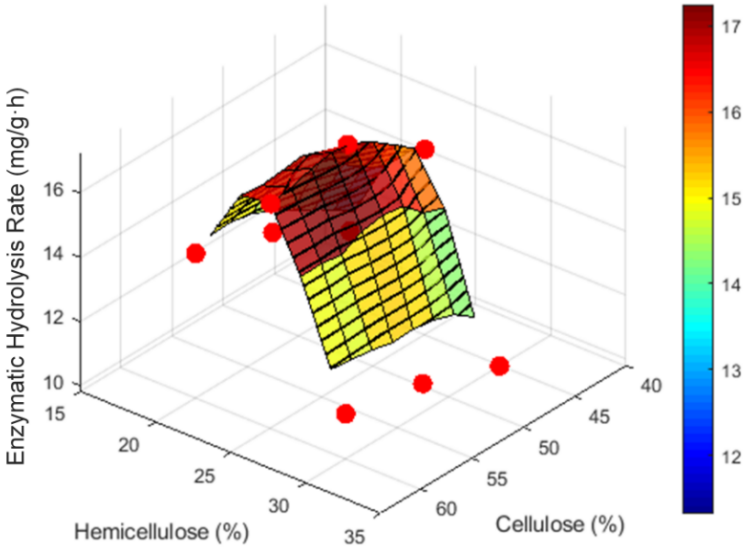

3.2 Dynamic control of multi-stage reaction conditions

The microwave-ultrasonic coupled pretreatment equipment has been developed. NIR spectroscopy is used to monitor the hemicellulose removal rate in real time. The reaction pH (5.2–6.8) and temperature (45–60°C) are automatically adjusted.

3.2.1 Microwave-Ultrasonic coupled pretreatment equipment design

The microwave-ultrasonic synergy improves the hemicellulose degradation rate by optimising the energy transfer efficiency. The equipment uses a dual-frequency composite reaction chamber with a microwave frequency of 2.45 GHz (with a continuously adjustable power of 0–1000 W) and an ultrasonic frequency of 20 kHz (pulse duty ratio of 10–90%). The energy coupling efficiency is solved by the Maxwell electromagnetic field equation and the acoustic pressure wave equation:

$$\begin{cases} \nabla \mathbf{H} = \sigma_d \mathrm{E}_d + \epsilon \dfrac{\partial \mathrm{E}_d}{\partial t} \\ \nabla^2 p - \dfrac{1}{c^2} \dfrac{\partial^2 p_s}{\partial t^2} = \rho_0 \dfrac{\partial q}{\partial t} \end{cases} \tag{6}$$

$\nabla \mathbf{H}$ is the magnetic field intensity. σ_d is the conductivity. E_d is the electric field intensity. $\nabla^2 p$ represents the Laplace operator of the sound pressure, which describes the propagation behaviour of ultrasound in the medium. p_s is the sound pressure. c is the sound speed. A three-dimensional multi-physics model is established using Cpmsol Multiphysics 6.1, and the geometric parameters of the reaction chamber are optimised to reduce the coefficient of variation of the energy density distribution.

The real-time impedance matching network is dynamically calibrated using the Smith chart to ensure that the microwave reflection power ratio is ≤5%. The ultrasonic transducer array uses phase modulation technology, and the sound intensity uniformity is regulated by Formula (7):

$$I_s = \frac{1}{N} \sum_{k=1}^{N} A_k^2 \sin^2 \left(\omega t + \phi_k \right) \tag{7}$$

It represents the synthetic sound intensity, reflecting the uniformity of the energy distribution of the ultrasonic wave in the reaction chamber. ω is the angular frequency. A_k^2 is the unit amplitude. ϕ_k is the phase compensation angle. This design reduces the dissociation energy of the lignin-carbohydrate complex, which is measured by differential scanning calorimetry.

Table 2 lists in detail the core operation parameters and technical indicators of the microwave-ultrasonic coupled pretreatment equipment. The system uses 2.45 GHz microwaves(Vectorscope model Keysight N5247B) and 20 kHz ultrasound to work together. The microwave power can be precisely adjusted within the range of 0–1000 W (±10 W). The ultrasonic pulse duty ratio can be controlled with a precision of ±2%. The key operating status is monitored in real time by a vector network analyser (microwave), a digital signal generator (ultrasonic frequency), and a high-speed data acquisition card. The reaction chamber pressure is maintained at 0.1–0.3 MPa (±0.01 MPa). Impedance matching efficiency ≥95% ensures efficient energy transmission. All parameters are collected online using industrial-grade sensors to provide a precise control basis for the multi-physics field coupling process. This configuration scheme is verified through multi-physics field simulation to meet the need for precise control of energy input in the biomass pretreatment process.

Table 2 Key operation parameters of the microwave-ultrasonic coupled pretreatment equipment

Parameter category	*Range/Specification*	*Control precision*	*Monitoring method*
Microwave frequency	2.45 GHz	±0.05 GHz	Vector network analyser
Microwave power	0–1000 W	±10 W	Directed coupler+power meter
Ultrasonic frequency	20 kHz	±0.5 kHz	Digital signal generator
Pulse duty ratio	10–90%	±2%	High-speed data acquisition card
Chamber pressure	0.1–0.3 MPa	±0.01 MPa	Piezoresistive pressure transducer
Impedance matching	≥95%	–	Reflected power ratio monitoring

Figure 3 intuitively presents the three-dimensional energy distribution characteristics with the synergistic effect of microwaves and ultrasound in the reaction chamber. The red area represents the high-energy area, and the blue area has lower energy. The energy density gradient change clearly reflects the coupling effect of the electromagnetic field and the acoustic field. The high-energy area is concentrated in the core area of the reaction chamber, forming an obvious energy focusing zone, which is in line with the theoretical expectation of the standing wave superposition principle. The energy attenuation trend in the edge area is significant, indicating that the equipment design effectively suppresses energy leakage and ensures the efficiency and stability of the pretreatment process. The overall uniformity of energy distribution verifies the optimisation effect of the composite reaction chamber. The phase-matching mechanism of microwaves and ultrasound successfully achieves balanced energy transfer in the spatial dimension. The local energy fluctuation is mainly caused by the phase mismatch between the electromagnetic field and the acoustic field. The reflection power ratio can be reduced by impedance calibration through the Smith circle diagram. Local energy fluctuation is inevitable in the pretreatment process, and its amplitude is controlled within the allowable range of system design, which will not significantly affect the overall reaction uniformity. Through phase modulation and impedance matching technology, the equipment has a good energy energy-stable output capacity, ensuring the consistency of pretreatment effect and process reliability. This distribution pattern provides a key basis for the subsequent process parameter optimisation, especially for the reaction time and temperature field control. In Figure 3, the colour transition is smooth, and there is no significant energy hole or abnormal peak, indicating that the equipment can maintain stable energy output under continuous operation. This visualisation result verifies the feasibility of the coupled pretreatment technology from an engineering perspective and lays a theoretical foundation for the reactor design in the industrial scale-up process.

Figure 3 Energy distribution of microwave-ultrasonic coupled pretreatment (see online version for colours)

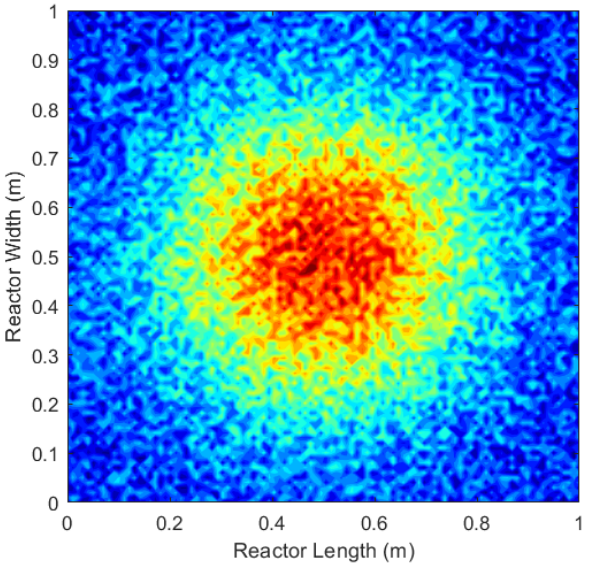

3.2.2 Near-infrared spectroscopy online monitoring and feedback control

The near-infrared (NIR) quantitative model is constructed with a spectral range of 4000–12,000 cm^{-1} and a resolution of 8 cm^{-1}. The spectral data are preprocessed using Savitzky-Golay smoothing (with a window width of 15 and second-order polynomials) combined with standard normal variable transformation. The prediction model for hemicellulose removal rate $\hat{b}$ uses PLSR:

$$\hat{b} = \sum_{i=1}^{n} w_i \cdot \mathrm{SNV}\left(\log\left(1/R\right)_{\lambda_i}\right) + b \tag{8}$$

SNV is the standard normal variable transformation (spectral preprocessing method). R is the reflectivity. w_i is the weight of the characteristic wavelength λ_i. b is the model bias term. Based on the NIR spectral data, the real-time removal rate of hemicellulose during the pretreatment process is predicted by PLSR to provide input for dynamic control. The root mean square error of model cross-validation is controlled within 8% to meet the requirements of industrial online monitoring accuracy.

The dynamic control system adopts the fuzzy proportional-integral-derivative (PID) algorithm. The input variable is the deviation between the NIR predicted value and the set value and its differential. The control rule library contains 81 Mamdani-type rules. The adjustment amount $\Delta u(t)$ of output pH and temperature is calculated as follows:

$$\Delta u(t) = K_p e(t) + K_i \int e(t)\,\mathrm{d}t + K_d \frac{\mathrm{d}e(t)}{\mathrm{d}t} \tag{9}$$

$e(t)$ is the deviation between the set value and the NIR predicted value. $\frac{de(t)}{dt}$ is the deviation change rate. Gain coefficients K_p, K_i, and K_d are optimised online through Lyapunov stability theory to ensure that the reaction system has less convergence time under disturbance. The actuator uses a high-precision metering pump (with a flow repeatability of ±0.5%) and a Peltier temperature control module (with a resolution of ±0.1°C) to achieve a certain pH fluctuation range (5.2–6.8) and temperature gradient (45–60°C).

This system can shorten the pretreatment time, improve the efficiency of cellulose enzymatic hydrolysis, and reduce the ratio of energy consumption of the coupled equipment, which meets the requirements of an industrial-grade scale-up economy.

The execution system parameter design in Table 3 is based on the dynamic response requirements of the biomass pretreatment process. The pH metering pump adopts a wide range adjustment capacity of 0.1–5.0 mL/min, which not only meets the initial rapid acid adjustment requirements (high flow) but also achieves fine control in the stable stage (low flow). Its response speed of <1 s can timely compensate for the pH fluctuation of the reaction system. The setting of the alkali solution concentration gradient (0.1–1.0 M NaOH) considers the differences in buffer capacity of different straw raw materials, and the mass flow closed-loop control ensures that the addition amount is precise to ±0.5%. The pulse width modulation (PWM) power regulation and the characteristic of fast response <30 s of the temperature module effectively solve the problem of local overheating in the microwave-ultrasonic coupling process. Nitrogen flow control (with a precision of ±0.2 L/min) prevents oxidation side reactions and avoids mass transfer obstacles caused by excessive inert gas. The control precision of ±5 rpm of the variable frequency stirring system (50–500 rpm) ensures mixing uniformity while avoiding damage from high shear forces to the fibre structure. The coordinated design of these parameters enables the system to adapt to fluctuations in raw material composition and provide an ideal physicochemical environment for subsequent enzymatic hydrolysis.

Table 3 Parameters of the actuator of the dynamic control system

Actuator unit	*Adjustment range*	*Response time*	*Control signal type*
pH metering pump	0.1–5.0 mL/min	<1s	4–20 mA PID output
Alkali tank concentration	0.1M–1.0M NaOH	–	Mass flow meter closed-loop control
Temperature control module	25–80°C	<30 s (90% setpoint)	PWM power regulation
Gas flow control	0–10 L/min (N_2)	±0.2 L/min	Mass flow controller
Stirring speed	50–500 rpm	±5 rpm	Frequency conversion motor+encoder feedback

3.3 Digital twin model construction

A virtual model of the industrial chain containing 37 key parameters (four modules: raw material properties, equipment operation, environmental constraints, and market dynamics) is established, and the GCN neural network is integrated to predict raw material supply fluctuations.

3.3.1 Multi-dimensional parametric modelling framework

In view of the complex characteristics of the agricultural waste resource industry chain, a virtual simulation system based on multi-scale modelling is constructed. Using the object-oriented modelling method, 37 key parameters are divided into four categories: raw material property parameters (8 items including moisture content, bulk density, cellulose content, hemicellulose content, lignin content, ash content, particle size distribution, and degradation rate), equipment operation parameters (11 items including processing capacity, power output, ultrasonic intensity, reaction temperature, pH precision, conveying speed, dust removal efficiency, failure rate, energy consumption coefficient, maintenance cycle, and vibration amplitude), environmental constraint parameters (9 items including collection radius, load limit, storage period, temperature and humidity requirements, subsidy policy, emission standard, noise limit, carbon allowance, and seasonal impact), and market dynamic parameters (9 items including raw material price, product price, demand cycle, inventory cost, transportation cost, labour cost, rental rate, financing rate, and carbon price). The coupling relationship between the parameters is represented by a directed acyclic graph (DAG), and the edge weight is quantitatively characterised by the Spearman rank correlation coefficient:

$$\rho_{ij} = 1 - \frac{6\sum d_k^2}{n\left(n^2 - 1\right)} \tag{10}$$

ρ_{ij} represents the rank correlation coefficient of parameters i and j. d_k^2 is the rank difference of the parameter pair. n is the sample size. The dynamic update mechanism of parameters adopts the sliding time window algorithm. The window width T_w is adaptively adjusted according to the parameter characteristics:

$$T_w = \frac{t_\tau}{\ln\left(\sigma_g / \sigma_0\right)} \tag{11}$$

t_τ is the parameter relaxation time. σ_g is the current observation standard deviation. σ_0 is the benchmark standard deviation. The model validation uses Sobol global sensitivity analysis to confirm the cumulative contribution rate of the top five dominant parameters to ensure that model simplification does not affect the prediction precision. Seasonal weight factors (1.5 for harvest period and 1.0 for the non-harvest period) are introduced in the window width adjustment to reflect the cyclical fluctuations of raw material supply.

3.3.2 Supply prediction driven by GCN

The graph convolutional neural network architecture is used in the raw material supply fluctuation prediction module, which innovatively integrates spatial topology and temporal features. The supply network graph is defined as $G = \left(V, E, W\right)$. V represents the collection point. The edge E represents the transportation path. The weight matrix W contains factors such as distance and traffic conditions. The node feature vector integrates 12-dimensional data such as historical supply and weather index. The graph convolution operation uses Chebyshev polynomial approximation:

$$Z = \sigma\left(\sum_{k=0}^{K}\theta_k T_k\left(\tilde{L}\right)X\right) \tag{12}$$

Z represents the node feature matrix after graph convolution. σ is the activation function. θ_k is the trainable weight parameter. X is the input node feature matrix, controlling the contribution of the polynomial term. $\tilde{L}$ is the normalised Laplace matrix. T_k is the *k*-order Chebyshev polynomial. Spatiotemporal feature extraction is achieved by stacking gated temporal convolution units:

$$H_t = \tanh\left(W_h * X_t + U_h * H_{t-1} + b_h\right) \tag{13}$$

H_t represents the hidden state at time step *t*. tanh is the hyperbolic tangent activation function. W_h is the convolution kernel weight of the current input X_t, which constrains the output range. * It is the convolution operation. U_h is the weight of the hidden state H_{t-1} at the previous time step. The prediction loss function uses Huber loss, which adaptively switches between mean-square error and absolute error:

$$L_\delta\left(y,\hat{y}\right) = \begin{cases} \frac{1}{2}\left(y-\hat{y}\right)^2, & \left|y-\hat{y}\right| \le \delta \\ \delta\left|y-\hat{y}\right| - \frac{1}{2}\delta^2, & otherwise \end{cases} \tag{14}$$

$L_\delta\left(y,\hat{y}\right)$ represents the loss between the predicted value and the actual value. δ is the threshold parameter. The curriculum learning strategy is adopted in the model training, gradually increasing the historical time step (12 → 36 → 72 weeks) and achieving a low root mean-square error of 8 weeks in advance on the dataset. This module improves the accuracy of raw material supply interruption risk warnings and supports dynamic scheduling decision-making.

Table 4 details the dimension configuration of the input features of the graph convolutional neural network and systematically shows the technical specifications of four key input features. The historical supply volume feature (3-dimensional) contains supply data of different time granularities and is updated daily. The meteorological data feature (4-dimensional) integrates environmental factors, such as temperature, precipitation, wind speed, and sunshine, and is updated every hour. The traffic condition feature (2-dimensional) reflects the logistics and transportation status in real time. The economic indicator feature (3-dimensional) covers market and policy elements and is updated weekly. This multi-dimensional feature engineering design ensures that the model can simultaneously obtain spatial topological relationships and temporal dynamic changes, providing a complete data foundation for graph convolution operations. The settings of all feature dimensions undergo strict variable screening and collinearity tests, which not only avoid information redundancy but also ensure the completeness of the feature space. The differentiated configuration of feature acquisition frequency fully considers the update characteristics of various types of data and the real-time requirements of the prediction task.

Table 4 GCN input feature dimensions

Feature type	*Dimensions*	*Data description*	*Collection frequency*
Historical supply	3	Daily/weekly/monthly supply volumes	Daily update
Meteorological data	4	Temperature, precipitation, wind speed, sunshine hours	Hourly update
Traffic conditions	2	Road congestion index, available transport vehicles	Real-time update
Economic indicator	3	Fuel price, labour cost, and policy incentive coefficient	Weekly update

3.4 Multi-node intelligent scheduling algorithm

A scheduling optimisation algorithm based on the improved NSGA-II is developed to achieve Pareto optimality between transportation cost and equipment vacancy rate.

3.4.1 Improved multi-objective optimisation framework of NSGA-II

Aiming to address the scheduling problem of the agricultural waste resource industry chain, an improved NSGA-II framework based on the elite strategy is constructed. The algorithm adopts a double-layer chromosome coding structure. The upper gene chain represents the transportation path planning, and integer coding is used to mark the access order of each node. The lower gene chain represents the equipment start-stop strategy. Binary coding is used to characterise the operating status of the pretreatment equipment and the bioreactor. The objective optimisation of transportation costs is as follows:

$$f_1 = \sum_{i=1}^{N}\sum_{j=1}^{M} c_{ij} x_{ij} d_{ij} \tag{15}$$

f_1 is the transportation cost, calculating the total cost of all transportation paths. c_{ij} is the transportation cost of unit distance. x_{ij} is the path selection variable. d_{ij} is the node spacing. Improvement strategies include the following:

1 *Dynamic crossover probability adjustment*: The crossover rate is adaptively adjusted based on population diversity indicators.

2 *Directed mutation operator*: Gaussian perturbations are applied to individuals with slow convergence speed in the non-dominated solution set. The mutation intensity is negatively correlated with the objective spatial distribution density.

The algorithm implements Pareto front classification through Fast Non-dominated Sort. The crowding distance comparison operator ensures the distribution of the solution set.

3.4.2 Constraint processing and real-time scheduling mechanism

A hybrid constraint satisfaction strategy is designed to handle three types of hard constraints: transport load limit, equipment minimum operation cycle, and time window requirements. A dynamic penalty function method is used to convert constraint violations into objective function correction terms:

$$\tilde{f}_i = f_i + \lambda_y \sum_{m=1}^{3} \max\left(0, G_m\right)^2 \tag{16}$$

$\tilde{f}_i$ is the corrected value of the i th objective function. The constraint violation is incorporated into the optimisation objective through the penalty function. f_i is the original value of the i th objective function. The penalty factor λ_y increases linearly with the number of iterations. G_m is the violation of the mth constraint condition. The initial value of the penalty factor in the dynamic penalty function method is set to 10, with an increase rate of doubling every 10 iterations. This setting is based on the results from earlier simulation experiments, which tested the balance between the algorithm's convergence speed and solution quality. It ensures sufficient exploration during early iterations while increasing the penalty for constraint violations in later stages to expedite convergence to the feasible solution region.

The real-time scheduling module is embedded in the rolling time domain optimisation architecture. The optimisation problem is resolved every 4 h. The equipment failure probability model is constructed based on historical data. The robustness compensation term is added to the objective function:

$$f_3 = \sum_{k=1}^{K} \rho_k \cdot \mathbb{E}\left[D_k\right] \tag{17}$$

f_3 is the expected capacity loss caused by equipment failure, quantifying the risk of equipment failure and enhancing the robustness of the scheduling scheme. ρ_k is the failure risk coefficient of equipment k. $\mathbb{E}\left[D_k\right]$ is the expected capacity loss. This mechanism shortens the scheduling adjustment response time with sudden failures and ensures the continuous and stable operation of the industrial chain.

The message passing interface (MPI) parallel computing framework is used in algorithm deployment, and the population size is set to 500. A single optimisation takes no more than 3 min on a 16-core server, meeting the timeliness requirements of actual engineering projects.

4 Method effect evaluation

4.1 NIR spectroscopy dynamic prediction and pH control performance

In the study of the performance of dynamic prediction of NIR spectroscopy and pH control, the data is from the real-time monitoring system of the microwave-ultrasonic coupled pretreatment equipment, including the spectral data of hemicellulose degradation process collected by the NIR spectrometer (4000–12,000 cm^{-1}, with a resolution of 8 cm^{-1}), and the dynamic reaction parameters recorded by the pH sensor. The study preprocesses the spectral data by Savitzky-Golay smoothing and standard normal variable transformation, establishes a PLSR model, and associates the characteristic wavelength with the hemicellulose removal rate. A fuzzy PID controller is also designed to dynamically adjust the pH and temperature using the spectral prediction value as the feedforward signal.

Figure 4 shows the synergistic mechanism of NIR spectroscopy real-time monitoring and dynamic pH control during agricultural waste pretreatment. The spectral curve of dynamic prediction of NIR spectroscopy reveals the characteristic changes of molecular vibration of hemicellulose degradation during microwave-ultrasonic coupling pretreatment. The intensity attenuation of the O-H second-order overtone peak (7000 cm^{-1}) directly reflects the degree of glycosidic bond breakage of hemicellulose. The spectral distortion of the C-H combination frequency region (8500–9500 cm^{-1}) characterises the dissociation state of the lignin-carbohydrate complex. The convergence of the PLSR correction curve and the original spectrum proves that the dynamic prediction model based on characteristic wavelength selection can effectively separate the target component signals in the mixed system and provide precise input for real-time control. In the fuzzy PID control response, the pH dynamic response curve with square wave excitation shows the control stability of the multi-physics field coupled system. The step change of the set value simulates the raw material fluctuation in actual production, and the rapid convergence characteristics of the system response are due to the precise modelling of the nonlinear mass transfer-reaction coupling process by the fuzzy rule base. The overshoot phenomenon reflects the instantaneous local acidification caused by the ultrasonic cavitation effect. The steady-state error range verifies the effectiveness of NIR feedforward compensation. The correlation between the dynamic prediction of infrared spectroscopy and the joint performance of pH control is reflected in the following aspect: the spectral characteristic peaks analyse the hemicellulose removal dynamics in real time, and its output is used as a feedforward signal to optimise the PID parameters, forming a closed-loop regulation of "spectral detection-model prediction-execution control". This joint control mechanism breaks through the control mismatch problem caused by detection lag in traditional pretreatment and realises the synchronous adaptation of reaction conditions and material changes.

4.2 Conversion efficiency improvement verification

High-performance liquid chromatography is used to detect the dynamic changes in reducing sugar yields with three treatments to quantitatively evaluate the performance advantages of the biocatalytic system. With corn straw as the uniform substrate, three parallel experiments are set up, including traditional dilute acid hydrolysis (1.2% H_2SO_4, 121°C), commercial cellulase preparation (Cellic CTec3, 10 FPU/g substrate), and the thermostable mutant enzyme system (BglM7 complex enzyme system) of this study. Chromatographic conditions include a mobile phase of 5mM H_2SO_4, with a flow rate of 0.6mL/min, a column temperature of 60°C, and a detector temperature of 55°C. Sample pretreatment follows the TP-510-42623 standard. Samples are taken every 8 h, and the reaction is terminated immediately. The samples are filtered through a 0.22μm microporous filter membrane before injection. The external standard method is used for the quantification of glucose and xylose. Data acquisition is completed using OpenLAB CDS 2.4 software, and multiple repeated measurements are set at each time point to control analytical errors. The dynamic model is fitted using the modification formula of the Michaelis-Menten equation. The cumulative saccharification rate within 72 h is calculated. One-way analysis of variance (ANOVA) is used for statistical significance tests. Tukey's honestly significant difference test (Tukey's HSD) is used for post hoc comparison.

Figure 4 NIR spectroscopy dynamic prediction and pH control joint performance (see online version for colours)

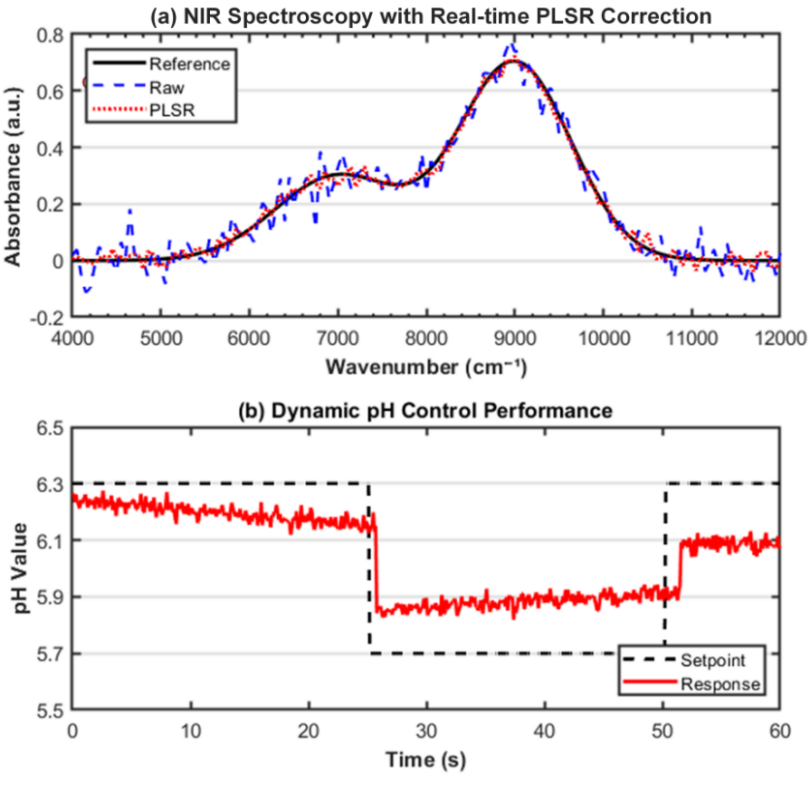

Figure 5 shows the dynamic changes in reducing sugar yields of three treatment methods (acid hydrolysis, commercial enzymatic hydrolysis, and mutant enzyme system) within 72 h and their statistical significance analysis. The reducing sugar yield results show that the initial hydrolysis rate of the acid hydrolysis method is relatively fast, and the final yield is only 60.8%, indicating that it is limited by the irreversible barrier of the lignin barrier. The commercial enzymatic hydrolysis method is more efficient, but the final yield is 81.4%, reflecting the insufficient stability of traditional enzymes. The mutant enzyme system maintains efficient conversion throughout the reaction cycle, with a final yield of 90.2% and no obvious plateau period, proving that its high-temperature resistance and continuous catalytic ability significantly improve the reaction efficiency. Statistical significance analysis is presented through heat maps. Tukey's HSD test is used to compare the three methods pairwise. The red area represents significant differences between the groups, and the symbol ** in the figure strengthens the time points with significant statistical differences ($p < 0.01$). The data show that all data statistics are significant, and the mutant enzyme system is significantly better than other methods at all time points. This change shows that the mutant enzyme effectively overcomes the limitations of traditional methods by optimising the active site structure, thereby maintaining efficient catalysis in long-term reactions. This result not only verifies the scientific value of the directed modification of biocatalysts but also provides a better technology path for the resource utilisation of agricultural waste.

Figure 5 Reducing sugar yield and statistical significance analysis (see online version for colours)

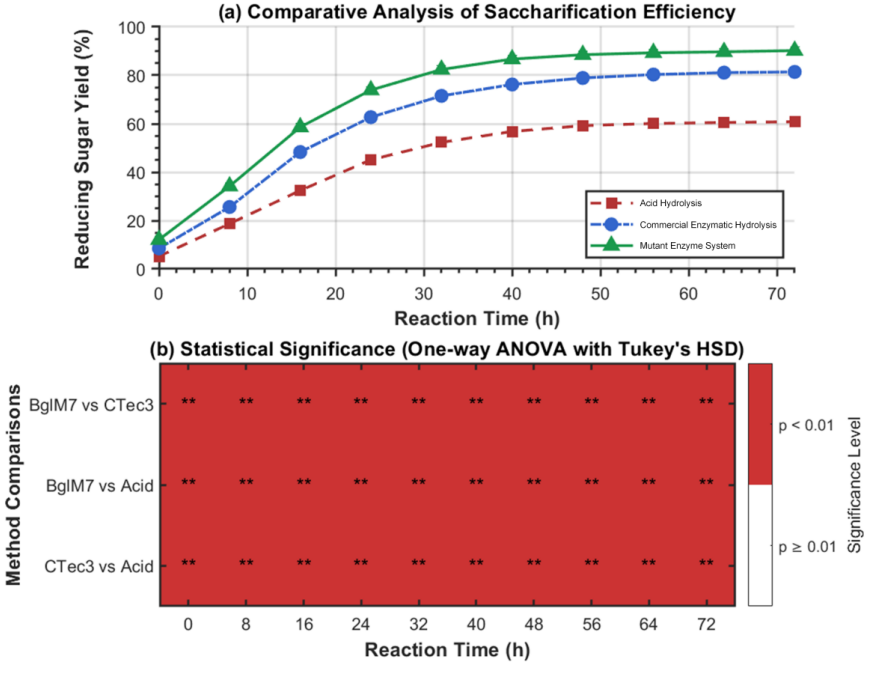

4.3 Scheduling cost analysis

The evaluation process focuses on the quantitative comparison of the optimisation rate of transportation paths and the loss of equipment vacancy. Three sets of comparison scenarios are constructed: digital twin dynamic scheduling system, manual experience scheduling (based on the decision records of practitioners with more than five years of experience), and fixed-route scheduling. The optimisation rate is defined as the deviation between the actual transportation distance and the theoretical shortest path:

$$\eta = 1 - \frac{\sum_{i=1}^{n} D_{\text{actual}}^{(i)}}{\sum_{i=1}^{n} D_{\text{optimal}}^{(i)}} \tag{18}$$

η is the optimisation rate. $D_{\text{actual}}^{(i)}$ is the actual path distance of the ith transportation. $D_{\text{optimal}}^{(i)}$ is the theoretical shortest path distance for the ith transportation. n is the total transportation batch. The calculation of equipment vacancy loss L_{idle} is:

$$L_{\text{idle}} = \sum_{k=1}^{K} \left(T_k^{\text{idle}} \cdot C_k^{\text{op}} \right) \tag{19}$$

K is the total number of equipment. T_k^{idle} is the vacancy time of equipment k. C_k^{op} is the unit time operating cost of equipment k. Data collection covers a 12-month operation cycle, integrating trajectory data, equipment operation logs, and order databases. A linear mixed effects model is used to control confounding factors, such as transportation

batches and seasonal fluctuations. Covariates include the fluctuation range of raw material moisture content, road network congestion index, and equipment maintenance cycle. All feature dimensions are tested for collinearity to ensure that there is no significant multicollinearity among features, so as to improve the stability and interpretability of the model.

Figure 6 compares the operation performance of the three scheduling strategies throughout the year, revealing the key advantages of the intelligent scheduling algorithm in the resource utilisation of agricultural waste. The horizontal axis represents the 12-month operation cycle, reflecting the impact of seasonal fluctuations on the scheduling strategy. The vertical axis represents the transportation path optimisation rate and equipment vacancy loss, respectively. The transportation path optimisation performance shows that the digital twin dynamic scheduling system (blue) always maintains a path optimisation rate of more than 0.8, which is significantly better than the manual experience scheduling (red) and the fixed-route scheme (green). This stability is due to the system's dynamic response ability to real-time traffic data, weather conditions, and fluctuations in raw material supply. Especially during the busy farming season, when the traditional method causes the optimisation rate to drop due to road network congestion, the digital twin system maintains efficient transportation through intelligent path replanning. The comparison of equipment utilisation efficiency further demonstrates that the digital twin system strictly controls the equipment vacancy loss within the range of US$21,000–23,000, which is significantly lower than traditional methods. This advantage is attributed to its precise scheduling capability based on demand prediction. By integrating equipment status monitoring and production task queue optimisation, the system significantly reduces the vacancy time of key equipment such as bioreactors. In contrast, although the fixed-route scheme has low loss, its rigid scheduling mode leads to the lowest optimisation rate throughout the year, and the static strategy is difficult to adapt to the seasonal fluctuations in agricultural waste collection. The digital twin system optimises equipment utilisation while improving transportation efficiency by coupling real-time data perception and intelligent decision-making algorithms. This collaborative optimisation is particularly important for the resource utilisation of agricultural waste – it not only reduces the cost of long-distance transportation of high-viscosity waste but also ensures the continuous operation of pretreatment equipment when the raw material supply is unstable. The research results provide key technical support for building a resilient supply chain and have practical significance for improving the economic feasibility of biomass energy projects.

4.4 Industrial chain coordination evaluation

The supply-demand matching index is used in the evaluation process to quantify the collaboration efficiency between the pretreatment centre and the biorefinery, which is defined as follows:

$$\mathrm{SMI} = 1 - \frac{\sum_{t=1}^{T} \left| D_t - S_t \right|}{2\sum_{t=1}^{T} \max\left(D_t, S_t \right)} \tag{20}$$

D_t is the daily demand of the biorefinery. S_t is the supply of the pretreatment centre. The data collection covers 365 days of operation records with three scheduling modes.

The Dagum Gini coefficient decomposition method is used to analyse the spatial-temporal dual-dimensional coordination differences. The SMI with each scheduling strategy is calculated.

Figure 6 Operation performance of scheduling algorithms (see online version for colours)

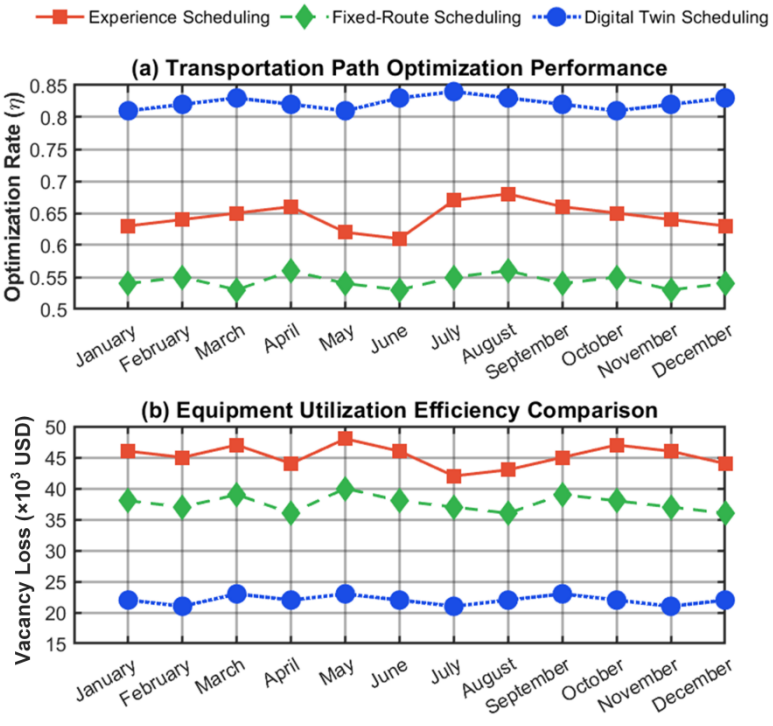

Figure 7 presents the full-year coordination efficiency performance of the three scheduling strategies in the agricultural waste resource industry chain. The vertical axis is the SMI, which quantifies the degree of operational coordination between the pretreatment centre and the biorefinery. Digital twin scheduling demonstrates significant advantages, with its SMI remaining high throughout the year with minimal fluctuations. This is due to its dynamic response mechanism, which can adjust transportation plans and equipment scheduling in real time and effectively respond to emergencies such as fluctuations in raw material supply and equipment failures. In contrast, the experience scheduling performs poorly, reflecting the limitations of relying on historical experience. The fixed-route scheduling (green) performs the weakest overall, with its rigid scheduling model unable to adapt to changes in supply and demand, experiencing a significant drop in efficiency during peak business hours. The differences between the three strategies are apparent, fully verifying the adaptability of the digital twin system in a complex operating environment. The data intuitively shows the key role of intelligent scheduling technology in improving the coordination efficiency of the industrial chain, reveals the inherent defects of traditional scheduling methods in dealing with seasonal fluctuations, and provides a clear decision-making basis for the optimisation and upgrading of

agricultural waste resource utilisation systems. The stability and adaptability of digital twin technology make it an important technical support for realising the circular economy of agriculture.

Figure 7 Supply chain coordination performance comparison (see online version for colours)

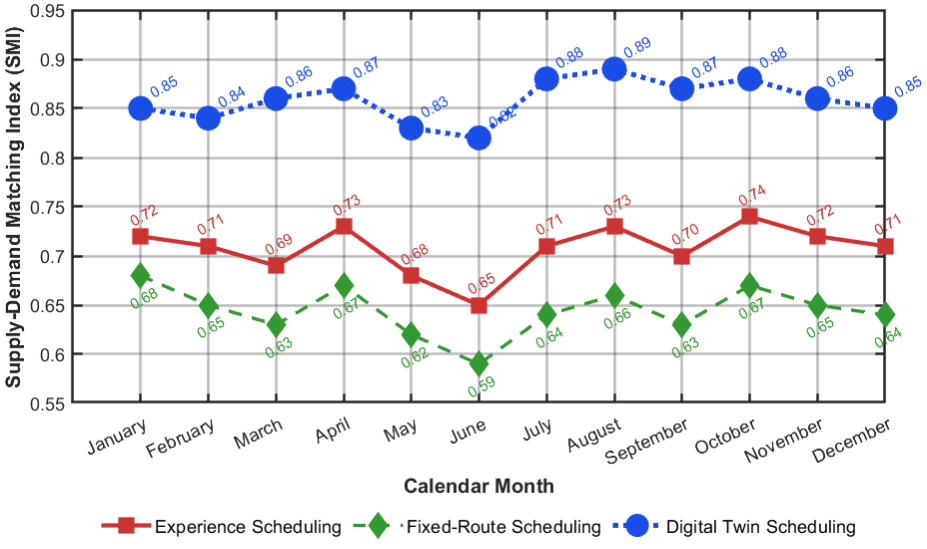

5 Conclusion

This study proposes and verifies the coordinated optimisation paradigm of the agricultural waste resource industry chain. Through the deep integration of biocatalytic system innovation and digital twin technology, the contradictions of low resource conversion efficiency, high operating costs, and insufficient industrial chain coordination in the traditional model are systematically solved. At the technology path level, the directed evolution technology based on the cellulase gene database breaks through the bottleneck of heat resistance of the biocatalyst and substrate adaptability, and the constructed enzyme system adaptation rules significantly improve the degradation efficiency of complex straw components. The microwave-ultrasonic coupled pretreatment equipment achieves precise control of the hemicellulose removal process through the synergistic effect of multi-physics fields. The digital twin model constructs a full-factor mapping of the industrial chain with 37 key parameters and combines the spatiotemporal feature extraction capabilities of graph convolutional neural networks to improve the precision of raw material supply prediction to industrial-grade practical standards. In terms of economic feasibility, the Pareto optimal solution set established by the improved NSGA-II algorithm between transportation costs and equipment utilisation verifies the economic advantages of multi-objective dynamic scheduling. The evaluation of the coordination of the industrial chain shows that the digital twin system improves the SMI compared with traditional models through a closed-loop decision-making mechanism driven by real-time data and improves its anti-interference ability. This ‘biological-digital’ dual-core-driven mode not only reduces the operating costs of the

entire life cycle but also strengthens the resilience of the industrial chain through multi-dimensional coupling optimisation. Policymakers can adjust the proportion of straw collection subsidies according to the fluctuation of carbon trading prices to balance economic and emission reduction benefits. This study provides a scalable technical and economic analysis framework for the resource utilisation of agricultural waste, and its methodology has a universal value for system optimisation in biomass energy, circular agriculture, etc. The current economic model has integrated the function of carbon price fluctuations and dynamic subsidy modules, initially demonstrating the significant impact of external policy tools on system economics. Further quantifying the synergistic effects between these two elements can provide scientific support for the government in formulating differentiated subsidy strategies and carbon quota allocation plans, thereby enhancing the market adaptability and long-term sustainability of agricultural waste resource projects. Therefore, future research should focus on large-scale engineering validation of technical systems and quantitative analysis of the coupling benefits between carbon trading mechanisms and policy subsidies.

Funding

This work was supported by 2025 Shandong Provincial Philosophy & Social Sciences Planning Project: Comprehensive Evaluation of the Competitiveness of Characteristic Rural Industry Clusters in Shandong and Strategies for Enhancement (Grant No. 25CGLJ28).

Conflicts of Interest

The authors declare no conflict of interest.

References

Ali, I., Islam, A., Ali, S.M. and Adnan, S. (2023) 'Identification and selection of suitable landfill sites using GIS-based multi-criteria decision analysis in the Peshawar District, Pakistan', *Waste Management and Research*, Vol. 41, No. 3, pp.608–619.

Alizadeh, P., Dumonceaux, T., Tabil, L.G., Mupondwa, E., Soleimani, M. and Cree, D. (2022) 'Steam explosion pre-treatment of sawdust for biofuel pellets', *Clean Technologies*, Vol. 4, No. 4, pp.1175–1192.

Åqvist, J. and van der Ent, F. (2022) 'Calculation of heat capacity changes in enzyme catalysis and ligand binding', *Journal of Chemical Theory and Computation*, Vol. 18, No. 10, pp.6345–6353.

Cai, Y., Yu, C., Zhu, X., Li, F., Zhou, H., Meng, C., Chen, H., Shen, Y., Tao, X. and Yuan, A. (2024) 'Synthesis of cheese-shaped capacitive covalent organic frameworks for lithium ion batteries by microwave ultrasonic coupling', *New Journal of Chemistry*, Vol. 48, No. 32, pp.14401–14409.

Capanoglu, E., Nemli, E. and Tomas-Barberan, F. (2022) 'Novel approaches in the valorization of agricultural wastes and their applications', *Journal of Agricultural and Food Chemistry*, Vol. 70, No. 23, pp.6787–6804.

Choi, H., Kim, Y.T., Tsang, Y.F. and Lee, J. (2023) 'Integration of thermochemical conversion processes for waste-to-energy: a review', *Korean Journal of Chemical Engineering*, Vol. 40, No. 8, pp.1815–1821.

Fawad, M., Ullah, F., Irshad, M., Shah, W., Mahmood, Q. and Ahmad, I. (2022) 'Marble waste site suitability assessment using the GIS-based AHP model', *Environmental Science and Pollution Research*, Vol. 29, No. 19, pp.28386–28401.

Gröger, H., Gallou, F. and Lipshutz, B.H. (2022) 'Where chemocatalysis meets biocatalysis: in water', *Chemical Reviews*, Vol. 123, No. 9, pp.5262–5296.

Gupta, G., Baranwal, M., Saxena, S. and Reddy, M.S. (2023) 'Utilization of banana waste as a resource material for biofuels and other value-added products', *Biomass Conversion and Biorefinery*, Vol. 13, No. 14, pp.12717–12736.

Gupta, N., Mahur, B.K., Izrayeel, A.M.D., Ahuja, A. and Rastogi, V.K (2022) 'Biomass conversion of agricultural waste residues for different applications: a comprehensive review', *Environmental Science and Pollution Research*, Vol. 29, No. 49, pp.73622–73647.

Hanefeld, U., Hollmann, F. and Paul, C.E. (2022) 'Biocatalysis making waves in organic chemistry', *Chemical Society Reviews*, Vol. 51, No. 2, pp.594–627.

He, X. (2024) 'An economic study on the resource utilization of agricultural waste', *Chinese Journal of Eco-Agriculture*, Vol. 32, No. 8, pp.1432–1440.

Hill, M., White, C., Wang, S., Thomas, J., Devincentis, B. and Singh, N. (2024) 'Computational fluid dynamics-based digital twins of fixed-bed bioreactors validate scaling principles for recombinant adeno-associated virus gene therapy manufacturing', *Biotechnology and Bioengineering*, Vol. 121, No. 9, pp.2662–2677.

Jha, S., Okolie, J.A., Nanda, S. and Dalai, A.K. (2022) 'A review of biomass resources and thermochemical conversion technologies', *Chemical Engineering and Technology*, Vol. 45, No. 5, pp.791–799.

Khalid, U., Rehman, Z.U., Ijaz, N., Khan, I. and Junaid, M.F. (2023) 'Integrating wheat straw and silica fume as a balanced mechanical ameliorator for expansive soil: a novel agri-industrial waste solution', *Environmental Science and Pollution Research*, Vol. 30, No. 29, pp.73570–73589.

Khanal, S., Karimi, K., Majumdar, S., Kumar, V., Verma, R., Bhatia, K.S., Kuca, K., Esteban, J. and Kumar, D. (2024) 'Sustainable utilization and valorization of potato waste: state of the art, challenges, and perspectives', *Biomass Conversion and Biorefinery*, Vol. 14, No. 19, pp.23335–23360.

Koksharov, S.A., Bikbulatova, A.A., Kornilova, N., Aleeva, S.V., Lepilova, O.V. and Nikiforova, E.N. (2022) 'Justification of an approach to cellulase application in the enzymatic softening of linen fabrics and clothing', *Textile Research Journal*, Vol. 92. Nos. 21–22, pp.4208–4229.

Lama, R. and Karmakar, S. (2024) 'Secure three-tier authentication approach for agricultural Internet of Things', *Cyber-Physical Systems*, Vol. 11, No. 3, pp.241–264.

Li, M., Zhou, C., Wang, B., Zeng, S., Mu, R., Li, G., Li, B. and Lv, W. (2023) 'Research progress and application of ultrasonic and microwave-assisted food processing technology', *Comprehensive Reviews in Food Science and Food Safety*, Vol. 22, No. 5, pp.3707–3731.

Liang, X., Li, X., Shu, L., Wang, X. and Luo, P. (2025) 'Tourism demand forecasting using graph neural network', *Current Issues in Tourism*, Vol. 28, No. 6, pp.982–1001.

Madhu, S., Devarajan, Y. and Natrayan, L. (2023) 'Effective utilization of waste sugarcane bagasse filler-reinforced glass fibre epoxy composites on its mechanical properties-waste to sustainable production', *Biomass Conversion and Biorefinery*, Vol. 13, No. 16, pp.15111–15118.

Mengqi, Z., Shi, A., Ajmal, M., Lihua, Y. and Awais, M. (2023) 'Comprehensive review on agricultural waste utilization and high-temperature fermentation and composting', *Biomass Conversion and Biorefinery*, Vol. 13, No. 7, pp.5445–5468.

Meraj, A., Singh, S.P., Jawaid, M., Nasef, M.M., Alomar, T.S. and AlMasoud, N. (2023) 'A review on eco-friendly isolation of lignin by natural deep eutectic solvents from agricultural wastes', *Journal of Polymers and the Environment*, Vol. 31, No. 8, pp.3283–3316.

Panasenko, A.E., Shichalin, O.O., Yarusova, S.B., Ivanets, A.I., Belov, A.A., Dran'kov, A.N., Azon, S.A., Fedorets, A.N., Buravlev, I.U., Mayorov, V.Y., Shlyk, D.K., Buravleva, A.A., Merkulov, E.B., Zarubina, N.V. and Papynov, E.K. (2022) 'A novel approach for rice straw agricultural waste utilization: synthesis of solid aluminosilicate matrices for cesium immobilization', *Nuclear Engineering and Technology*, Vol. 54, No. 9, pp.3250–3259.

Park, S.Y., Kim, S.J., Park, C.H., Kim, J. and Lee, D.Y. (2023) 'Data-driven prediction models for forecasting multistep ahead profiles of mammalian cell culture toward bioprocess digital twins', *Biotechnology and Bioengineering*, Vol. 120, No. 9, pp.2494–2508.

Pažitný, A., Halaj, M., Russ, A., Boháček, S., Ihnát, V., Skotnicová, I. and Šutý, S. (2022) 'Steam explosion and steam extrusion pretreatment as auxiliary methods for concentration enhancement of monosaccharides from hydrolysates based on the selected lignocellulosic materials', *Monatshefte Für Chemie-Chemical Monthly*, Vol. 153, No. 11, pp.1077–1085.

Peng, X., Jiang, Y., Chen, Z., Osman, A.I., Farghail, M., Rooney, D.W. and Yap, P.S. (2023a) 'Recycling municipal, agricultural and industrial waste into energy, fertilizers, food and construction materials, and economic feasibility: a review', *Environmental Chemistry Letters*, Vol. 21, No. 2, pp.765–801.

Peng, X., Gai, S., Cheng, K. and Yang, F. (2023b) 'Hydrothermal humification mechanism of typical agricultural waste biomass: a case study of corn straw', *Green Chemistry*, Vol. 25, No. 4, pp.1503–1512.

Phiri, R., Rangappa, S.M., Siengchin, S.,Oladijo, O.P. and Dhakal, H.N. (2023) 'Development of sustainable biopolymer-based composites for lightweight applications from agricultural waste biomass: a review', *Advanced Industrial and Engineering Polymer Research*, Vol. 6, No. 4, pp.436–450.

Rui, G. and Li, M. (2024) 'Utilizing internet big data and machine learning for product demand forecasting and analysis of its economic benefits', *Tehnički Vjesnik*, Vol. 31, No. 4, pp.1385–1394.

Semwal, S., Sivagurunathan, P., Satlewal, A., Kumar, R., Gupta, R.P., Christopher, J. and Kumar, R. (2024) 'An efficient and cost-effective pretreatment of rice straw using steam explosion: a pilot scale experience', *Waste and Biomass Valorization*, Vol. 15, No. 4, pp.1975–1986.

Srivastava, N., Mohammad, A., Pal, D.B., Srivastava, M., Alshahrani, M.Y., Ahmad, I., Singh, R., Mishra, P.K., Yoon, T. and Gupta, V.K. (2024) 'Enhancement of fungal cellulase production using pretreated orange peel waste and its application in improved bioconversion of rice husk under the influence of nickel cobaltite nanoparticles', *Biomass Conversion and Biorefinery*, Vol. 14, No. 5, pp.6687–6696.

Toma, D.I., Baroi, A.M., Vizitiu, D.E., Din, A., Fierascu, I. and Fierascu, R.C. (2024) 'Grapevine plant waste utilization in nanotechnology', *AgroLife Scientific Journal*, Vol. 13, No. 1, pp.203–216.

Tu, Y., Li, W., Song, X., Gong, K., Liu, L., Qin, Y., Liu, S. and Liu, M. (2024) 'Using a graph neural network to conduct supplier recommendation based on a large-scale supply chain', *International Journal of Production Research*, Vol. 62, No. 24, pp.8595–8608.

Yalcinkaya, S. and Uzer, S. (2022) 'A GIS-based multi-criteria decision support model for planning municipal solid waste collection points: a case study of çağdaş neighbourhood, Çiğli district, Izmir, Turkey', *Waste Management and Research*, Vol. 40, No. 8, pp.1297–1310.

Zhang, R., Cao, C., Bi, J., Li, Y. (2022) 'Fungal cellulases: protein engineering and post-translational modifications', *Applied Microbiology and Biotechnology*, Vol. 106, No. 1, pp.1–24.

Zheng, F., Hou, S., Xue, L., Yang, W. and Zhan, C.G. (2023) 'Human butyrylcholinesterase mutants for (−)-'cocaine hydrolysis: a correlation relationship between catalytic efficiency and total hydrogen bonding energy with an oxyanion hole', *The Journal of Physical Chemistry B*, Vol. 127, No. 50, pp.10723–10729.

Zhu, Y., Wen, X. and Guo, Z. (2025) 'Research progress on high-value utilization technology of sludge solid waste in China', *Journal of Material Cycles and Waste Management*, Vol. 27, No. 1, pp.654–665.